





## Research Article

# The Numerical Investigation of the Heat Transport in the Nanofluids under the Impacts of Magnetic Field: Applications in Industrial Zone

Adnan <sup>1</sup>, Umar Khan <sup>2</sup>, Naveed Ahmed,<sup>3</sup> Syed Tauseef Mohyud-Din,<sup>4</sup> Ilyas Khan <sup>5</sup>,  
and Md. Fayz-Al-Asad <sup>6</sup>

<sup>1</sup>Department of Mathematics, Mohi-ud-Din Islamic University, Nerian Sharif AJ&K 12080, Trarkhel, Pakistan

<sup>2</sup>Department of Mathematics and Statistics, Hazara University, Mansehra 21120, Pakistan

<sup>3</sup>Department of Mathematics, Faculty of Sciences, HITEC University, Taxila Cantt 47070, Taxila, Pakistan

<sup>4</sup>University of Multan, Multan 66000, Pakistan

<sup>5</sup>Department of Mathematics, College of Science Al-Zulfi, Majmaah University, Al-Majmaah 11952, Saudi Arabia

<sup>6</sup>Department of Mathematics, Bangladesh University of Engineering and Technology (BUET), Dhaka 1000, Bangladesh

Correspondence should be addressed to Md. Fayz-Al-Asad; fayzmath.buet@gmail.com

Received 25 May 2021; Accepted 18 July 2021; Published 28 July 2021

Academic Editor: Gengxin Sun

Copyright © 2021 Adnan et al. This is an open access article distributed under the Creative Commons Attribution License, which permits unrestricted use, distribution, and reproduction in any medium, provided the original work is properly cited.

The dynamics of the nanofluid flow between two plates that are placed parallel to each other is of huge interest due to its numerous applications in different industries. Keeping in view the significance of such flow, investigation of the heat transfer in the Cu-H<sub>2</sub>O nanofluid is conducted between parallel rotating plates. For more significant results of the study, the squeezing effects are incorporated over the plates that are electrically conducting. The nondimensional flow model is then treated analytically (VPM), and the results are sketched against the preeminent flow parameters. The remarkable heat transfer in the nanofluid is noticed against the Eckert and Prandtl numbers, whereas the Lorentz forces oppose the fluid temperature. Furthermore, the shear stresses at the walls drop and the local heat transfer rate rises due to increasing flow parameters. Finally, to validate the study, a comparison is made with existing available science literature and noted that the presented results are aligned with them.

## 1. Introduction

The heat transport investigation in the squeezed flow is substantial for engineering and industrial view point. These are in cooling, fog formation, lubrication system, food processing, and hydrodynamical machines etc. In view of significance of the squeezed flow, researchers and scientists focused to analyze the flow behavior and thermal performance under multiple flow conditions. Firstly, the squeezed flow of lubricants was introduced in [1].

Mustafa et al. [2] pointed out the flow behavior in fluids squeezed between two plates. The influence of multiple preeminent flow parameters on the fluid temperature and mass transport is decorated via graphs and explained comprehensively. Moreover, they found the local thermal

performance against ingrained flow parameters. The analysis of magnetized flow regimes by considering the suction/blowing characteristics is imperative. It strengthens roots in civil engineering and industries as well. The analytical investigation of the fluid squeezed between parallel disks with suction/blowing characteristics was perceived in [3]. Further, they analyzed the flow characteristics under varying multiple parameters. The flow of H<sub>2</sub>O composed by the Cu nanomaterial was presented by Khan et al. [4]. To enhance the thermal performance in the fluid, they adopted thermal conductance correlation based on multiple geometries of the nanomaterial. They pointed out that thermal performance is prompt for the platelet nanomaterial-based nanofluid.

The thermal transport analysis in the colloidal mixture between the opening/narrowing channel was detected in [5].

The walls of the channel are flexible and with source/sink situated at the culmination of the wall. For novelty of the colloidal model, they ingrained the impact of Lorentz forces in the energy equation. The enhanced thermal conductance of the fluid by dispersing nanomaterial, nanotubes, and various thermal conductance correlations was perceived in [6–8]. In 2014, Goktepe et al. [9] performed comparative inspection between single- and two-phase nanofluid models with convection characteristics. The thermal transport inspection in the unsteady colloidal mixture between parallel plates was perceived in [10]. They conducted the analysis between magnetized plates and decorated the results for the flow regimes. The most relevant investigation in the colloidal mixtures composed by various types of nanomaterials suspended in different host liquids was presented in [11–14].

Dogonchi et al. [15] inspected the temperature behavior in the magnetized nanofluid with radiative heat flux effects. They found that the temperature of the nanofluid enhanced against stronger thermal radiative effects. Further, the enhanced local thermal performance rate was reported in the work for the higher thermal radiation parameter. An analytical treatment of the nanofluid bounded by parallel plates was carried out in [16]. They used the Brownian motion effects, and to enhance the thermal performance in the used colloidal mixture, KKL thermal conductance correlation was ingrained in the energy equation. They pointed out that the local heat transport rate rises against higher volume fraction of the tiny material. Sheikholeslami et al. [17] perceived Brownian motion and thermophoretic effects on the flow characteristics. They revealed that the shear stresses at the plate surface enhanced for higher Hartmann and viscosity parameters. Also, they validated the analysis via comparative analysis.

The thermal and mass transport analysis in the colloidal mixture between rotating plates was perceived in [18]. Further, they revealed that the heat transport is in direct proportion for thermophoresis and Brownian motion parameters, while reverse behavior is pointed out for the concentration field. Singh et al. [19] pointed out the heat and mass transportation in the squeezed flow by imposing the slip effects on the plates. Also, they incorporated the influence of Lorentz forces and explored the significant results. They revealed that the heat and mass transport at the plate surface reduced against high Lorentz forces and volume fraction. Further, increment in the mass transport was detected against Schmidt and squeeze numbers. A novel thermal transport in GO-Molybdenum-disulfide/H<sub>2</sub>O-C<sub>2</sub>H<sub>6</sub>O<sub>2</sub> was reported in [20]. They conducted the analysis between parallel rotating plates and found the significant results for the thermal performance of the hybrid nanofluid. To improve the thermal performance rate, they ingrained the Cattaneo–Christov model in the energy relation and perceived significant changes in the heat transfer rate. Further, significant heat transfer investigation in the nanofluids was detected in [21, 22].

In 2019, Shah et al. [23] performed the analysis of heat and mass transport in rotating geometry. For novel analysis, they ingrained the radiative heat flux and Hall current in the energy and momentum constitutive relations. They decorated the results against the flow parameters and explained comprehensively. Recently, Khan et al. [24] conducted the thermal transportation over a sensor surface for  $\gamma$ -nanofluids. For thermal enhancement of the fluid, they adopted the effective Prandtl model and revealed significant changes in the thermal and momentum transport. Recently, Gul et al. [25] revealed the nanofluid thermal transport against the upright channel through the permeable medium. They highlighted the flow behavior for different parameters and described comprehensively.

The thermal transport analysis between parallel plates is significant. From the literature visit, it is revealed that the thermal performance in the nanofluids composed by multiple nanomaterials geometries is not conducted so far. Such thermal analysis is imperative for industrial and engineering view point. Therefore, the magnetized flow of H<sub>2</sub>O composed by multiple nanomaterials (platelets, blades, and cylinders) is organized. For the mathematical study, variation of parameters method (VPM) is adopted, and it successfully tackled the colloidal model. The results for thermal performance, shear stresses, and local heat transfer rate against multiple flow parameters are decorated and explained comprehensively. A comparative investigation is also conducted, which proved the reliability of the adopted technique. Finally, core results of the analysis are ingrained in the conclusion section.

## 2. Materials and Methods

### 2.1. Model Formulation

**2.1.1. Model Description and Geometry.** The unsteady and electrically conducting fluid is taken between two parallel rotating plates in the Cartesian coordinate frame. A thermal conductance correlation based on multiple nanomaterial geometries is taken to improve the thermal performance of the model. The plates are apart from  $z = \pm l[1 - \alpha t]^{1/2} = \pm h(t)$ , where  $\alpha > 0$  and  $t < 1/\alpha$ . Further, dissipation effects are plugged in the energy relation. The following restrictions are imposed on the colloidal flow model.

The flow is incompressible.

The volumetric fraction of the nonmaterial and the regular substance are thermally compatible.

There are no slip effects between them.

There is no chemical reaction occurring.

Figure 1 depicts the flow configuration of the Cu-H<sub>2</sub>O nanofluid. In the view of aforementioned restrictions, the colloidal model which governs the flow of Cu-H<sub>2</sub>O for multiple geometries of the nanomaterial takes the following form:

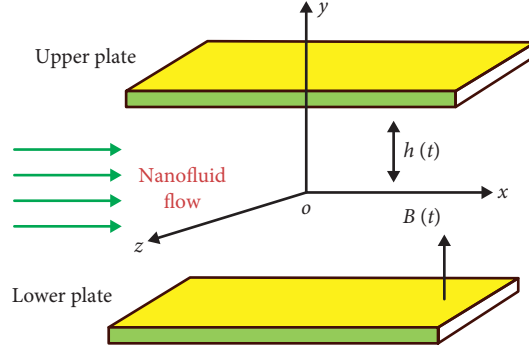


FIGURE 1: Geometry of the flow.

$$\frac{\partial u}{\partial x} + \frac{\partial v}{\partial y} = 0, \quad (1)$$

$$\rho_{nf} \left( \frac{\partial u}{\partial t} + u \frac{\partial u}{\partial x} + v \frac{\partial u}{\partial y} \right) = -\frac{\partial p}{\partial x} + \mu_{nf} \left( \frac{\partial^2 u}{\partial x^2} + \frac{\partial^2 u}{\partial y^2} \right) - \frac{\sigma_{nf} B_0^2}{\rho_{nf}} u, \quad (2)$$

$$\rho_{nf} \left( \frac{\partial v}{\partial t} + u \frac{\partial v}{\partial x} + v \frac{\partial v}{\partial y} \right) = -\frac{\partial p}{\partial y} + \mu_{nf} \left( \frac{\partial^2 v}{\partial x^2} + \frac{\partial^2 v}{\partial y^2} \right), \quad (3)$$

$$\left( \frac{\partial T}{\partial t} + u \frac{\partial T}{\partial x} + v \frac{\partial T}{\partial y} \right) = \frac{k_{nf}}{(\rho C_p)_{nf}} \left( \frac{\partial^2 T}{\partial x^2} + \frac{\partial^2 T}{\partial y^2} \right) + \frac{\mu_{nf}}{(\rho C_p)_{nf}} \left( 4 \left( \frac{\partial u}{\partial x} \right)^2 + \left( \frac{\partial u}{\partial y} \right)^2 + \left( \frac{\partial v}{\partial x} \right)^2 \right). \quad (4)$$

And, supporting boundary conditions are

$$v = \frac{\partial u}{\partial y} = \frac{\partial T}{\partial y} = 0 \text{ at } y = 0, \quad (5)$$

$$v = v_w = \frac{dh}{dt}, T = T_H \text{ at } y = h(t). \quad (6)$$

Equation (1) is the conservation of mass, and the velocities along the coordinate axes are represented by  $u$  and  $v$ , respectively,  $p$  is the pressure, and  $T$  is the temperature. To enhance the flow characteristics, following correlations are adopted [26, 27]:

$$\rho_{nf} = (1 - \phi)\rho_f + \phi\rho_s, \quad (7)$$

$$\mu_{nf} = \frac{\mu_f}{(1 - \phi)^{2.5}}, \quad (8)$$

$$(\rho C_p)_{nf} = (1 - \phi)(\rho C_p)_f + \phi(\rho C_p)_s, \quad (9)$$

$$\sigma_{nf} = \sigma_f \left( 1 + \frac{3(\sigma_s/\sigma_f - 1)\phi}{(\sigma_s/\sigma_f + 2) - (\sigma_s/\sigma_f - 1)\phi} \right). \quad (10)$$

For thermal improvement, the following model is used [16]:

$$k_{nf} = k_f \left( \frac{k_s + (m - 1)k_f - (m - 1)(k_f - k_s)\phi}{k_s + (m - 1)k_f + (k_f - k_s)\phi} \right), \quad (11)$$

where conductivity of the tiny particles, regular liquid, and shape factor of the nanoparticles are denoted by  $k_s$ ,  $k_f$ , and  $m$ , respectively. The shape factor of the tiny particles is computed by  $3/\psi$ .

The appropriated dimensionless transforms are described by the following formulas in which  $\eta$  is similarity variables in which the fluid is squeezed for  $\alpha > 0$  and  $t < 1/\alpha$ . The flow is squeezed between the plates until the time reaches the limit  $1/\alpha$ . Further,  $u$ ,  $v$ , and  $T$  describe the velocities along horizontal, vertical, and the temperature, respectively:

$$\eta = \frac{y}{l(1 - \alpha t)^{1/2}}, u = \frac{\alpha x}{2(1 - \alpha t)} F'(\eta), v = -\frac{\alpha l}{2(1 - \alpha t)^{1/2}} F(\eta), T = T_H \theta(\eta). \quad (12)$$

After using these variables in equations (1)–(4) and plugging the partial differentiations and self-similar variables, the following nanofluid model is attained:

$$F'''(\eta) - SK_1(1 - \phi)^{2.5} \left( \eta F'''(\eta) + F'(\eta) F''(\eta) - F(\eta) F'''(\eta) + 3F''(\eta) \right) - \frac{MA_1}{(1 - \phi)^{2.5}} F''(\eta) = 0, \tag{13}$$

$$\theta''(\eta) + \frac{PrSK_2}{K_3} (\theta'(\eta) F(\eta) - \eta \theta'(\eta)) + \frac{PrEc}{K_3(1 - \phi)^{2.5}} \left( F''^2(\eta) + 4\delta^2 F'^2(\eta) \right) = 0. \tag{14}$$

The reduced dimensionless conditions at the plates are labeled in equations (15) and (16), respectively. It is noteworthy to mention that  $\eta = 0$  and  $\eta = 1$  denote the conditions at the lower and upper plates, respectively:

$$F(0) = 0, F''(0) = 0, F(1) = 1, F'(1) = 0, \tag{15}$$

$$\theta'(0) = 0, \theta(1) = 1. \tag{16}$$

In equations (13) and (14), squeeze, Prandtl, Eckert, and Hartmann numbers are denoted by  $S = \alpha l^2 / 2\nu_f$ ,  $Pr = \mu_f (\rho C_p)_f / \rho_f k_f$ ,  $Ec = \rho_f l / (\rho C_p)_f (\alpha x / 2(1 - \alpha t))^2$ ,  $M = lB_0 (\sqrt{\sigma_f(1 - \alpha t)} / \mu_f)$ , and  $\delta = l/x$ . The quantities represented by  $K_1, K_2, K_3$ , and  $A_1$  are equal to

$$K_1 = (1 - \phi) + \frac{\phi \rho_s}{\rho_f}, \tag{17}$$

$$K_2 = (1 - \phi) + \frac{\phi (\rho C_p)_s}{(\rho C_p)_f}, \tag{18}$$

$$K_3 = \left( \frac{k_s + (m - 1)k_f - (m - 1)(k_f - k_s)\phi}{k_s + (m - 1)k_f + (k_f - k_s)\phi} \right), \tag{19}$$

$$A_1 = \left( \frac{(\sigma_s + 2\sigma_f) + 2(\sigma_s - \sigma_f)\phi}{(\sigma_s + 2\sigma_f) - (\sigma_s - \sigma_f)\phi} \right). \tag{20}$$

The dimensional formulas for the shear stresses and Nusselt number are  $C_F = \mu_{nf} (\partial u / \partial y)_{y=h(t)} / \rho_{nf} v_w^2$  and  $Nu = -lk_{nf} (\partial T / \partial y)_{y=h(t)} / KT_H$ .

After some calculations, these expressions become

$$C_F = K_1(1 - \phi)^{2.5} F''(1), \tag{21}$$

$$Nu = -K_3 \theta'(1). \tag{22}$$

**2.2. Mathematical Analysis.** As under consideration, the nanofluid model is highly nonlinear in nature, and a closed form of the solution is very tedious or do not exist in general

for such models. Therefore, we then move to tackle the model approximately. For the said purpose, the method known as variation of parameters method [28] is used. Primarily, the method is based on the Lagrange multiplier which can be calculated according to the model. After that, a recursive relation is written for the velocity and temperature equations. The initial conditions are used to calculate the initial guess, and the boundary conditions are used to compute the remaining constants appearing in the recursive relation. The detailed implementation of the method is given below.

**2.2.1. Working Rules for VPM**

Step 1: the initial step in VPM [28] is to reduce the nonlinear model in the following form:

$$\widehat{\mathcal{L}} \widehat{\mathcal{F}}(\eta) + \widehat{\mathcal{R}} \widehat{\mathcal{F}}(\eta) + \widehat{\mathcal{N}} \widehat{\mathcal{F}}(\eta) + \widehat{\mathcal{G}}^*(\eta) = 0, \tag{23}$$

where the highest order linear operator is  $\widehat{\mathcal{L}}$ ,  $\widehat{\mathcal{R}}$  is also the linear operator with order less than  $\widehat{\mathcal{L}}$ ,  $\widehat{\mathcal{N}}$  presents the nonlinear operator, and  $\widehat{\mathcal{G}}^*$  is the inhomogeneous part of the model.

Step 2: it is the calculation of the Lagrange Multiplier. For VPM, the Lagrange multiplier is calculated by adopting the following formula:

$$\lambda(s, \eta) = \frac{(-1)^{n^*} (\eta - s)^{n^* - 1}}{(n^* - 1)!}. \tag{24}$$

In equation (24),  $n^*$  signifies the highest order derivative in the model.

Step 3: it is the calculation of initial approximation for the model. The initial approximation is calculated by means of initial conditions by adopting the following formula:

$$\mathcal{F}_0(\eta) = \sum_{i=0}^k \frac{\eta^i \mathcal{F}^i(0)}{i!}. \tag{25}$$

Step 4: it is the construction of the iterative scheme for VPM. The scheme is constructed by the following way:

$$\mathcal{F}_{n+1}(\eta) = \mathcal{F}_0(\eta) + \int_0^\eta \lambda(s, \eta) (-\mathfrak{R}\mathcal{F}(s) - \mathfrak{N}\mathcal{F}(s) - g^*(s)) ds, \quad n \geq 0. \tag{26}$$

By plugging the initial approximation and Lagrange multiplier, higher order approximations can be computed by running the recursive iterated scheme given in equation (26).

2.3. *Implementation of the Proposed Technique.* In VPM, equations (13) and (14) take the following form of recurrence relation:

$$F_{n+1}(\eta) = F(0) + F'(0)\eta + F''(0)\frac{\eta^2}{2!} + F'''(0)\frac{\eta^3}{3!} - \int_0^\eta \frac{(\eta - \check{s})^3}{3!} \left[ -SK_1(1 - \phi)^{2.5} \left( \check{s}F'''(\check{s}) + 3F''(\check{s}) + F'(\check{s})F''(\check{s}) - F(\check{s})F'''(\check{s}) \right) - MA_1(1 - \phi)^{2.5}F''(\check{s}) \right] d\check{s}, \tag{27}$$

$$\theta_{n+1}(\eta) = \theta(0) + \eta\theta'(0) - \int_0^\eta (\eta - \check{s}) \left[ \frac{PrSK_2}{K_3} (F(\check{s})\theta'(\check{s}) - \check{s}\theta'(\check{s})) + \frac{PrEc}{K_3(1 - \phi)^{2.5}} \left( F''^2(\check{s}) + 4\delta^2 F'^2(\check{s}) \right) \right] d\check{s}. \tag{28}$$

After plugging the conditions in equations (27) and (28), the following relations are obtained:

$$F_{n+1}(\eta) = \check{C}_1\eta + \frac{\check{C}_2\eta^3}{6} - \int_0^\eta \frac{(\eta - \check{s})^3}{3!} \left[ -SK_1(1 - \phi)^{2.5} \left( \check{s}F(\check{s}) + 3F(\check{s}) + F'(\check{s})F(\check{s}) - F(\check{s})F'''(\check{s}) \right) - MA_1(1 - \phi)^{2.5}F''(\check{s}) \right] d\check{s}, \tag{29}$$

$$\theta_{n+1}(\eta) = C_3 + C_4\eta - \int_0^\eta (\eta - \check{s}) \left[ \frac{PrSK_2}{K_3} (F(\check{s})\theta'(\check{s}) - \check{s}\theta'(\check{s})) + \frac{PrEc}{K_3(1 - \phi)^{2.5}} \left( F'^2(\check{s}) + 4\delta^2 F'^2(\check{s}) \right) \right] d\check{s}, \tag{30}$$

where  $\check{C}_i$  for  $i = 1, \dots, 4$  are constants and computed by plugging the remaining flow conditions. Table 1 presents the comparative computation between VPM solutions and numerical computations.

### 3. Results and Discussion

3.1. *The Velocity Field.* The analysis of the imposed magnetic field on the flow of nanofluids is significant as it is used in many industrial products to purify the products. Therefore, the nanofluid motion against the Hartmann number is presented in Figures 2(a) and 2(b) for  $F(\eta)$  and  $F'(\eta)$ , respectively. It is noticed that the fluid velocity  $F(\eta)$  reduces by strengthening the magnetic field. Physically, the applied magnetic field opposes the fluid movement due to which the fluid motion declines. On the contrary, dual behavior of the fluid motion is observed for the velocity component  $F'(\eta)$ . Further, from the plotted results, it is obvious that the fluid motion declines and rises almost inconsequentially against the imposed magnetic field.

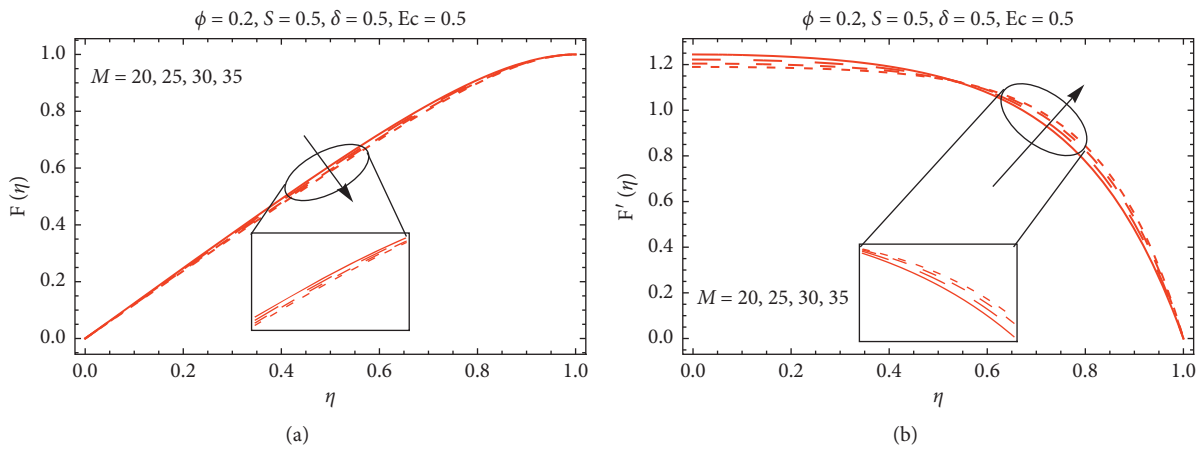
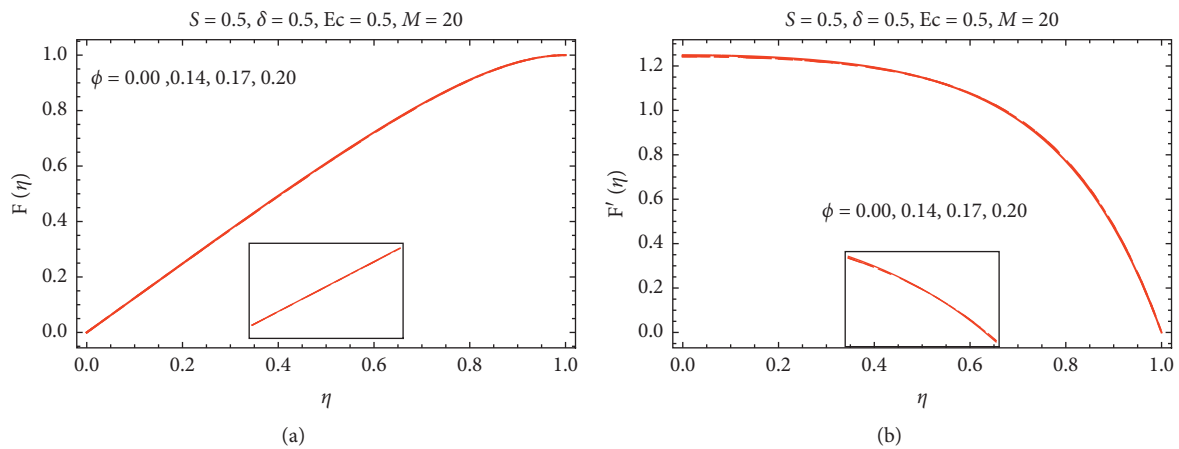
Figures 2 and 3 elaborate the fluid velocities  $F(\eta)$  and  $F'(\eta)$  for increasing values of volumetric fraction of Cu nanoparticles and squeezing parameter. From Figure 3, it is observed that the velocity components alter almost

inconsequentially due to varying  $\phi$ . Physically, by increasing the volume fraction of Cu nanoparticles, the resultant colloidal fluid becomes more denser which leads to slow movement of the fluid. The effects of the squeezing parameter on the velocities are demonstrated in Figure 4. It is noticed that the variations in the fluid motion are not prominent due to increasing squeezing effects. The values of thermophysical parameters are described in Table 2.

3.2. *Temperature Field.* The behavior of fluid temperature against multiple values of  $\phi$  and Pr is plotted in Figure 5. These results are plotted for different nanoparticle shapes, namely, platelets, cylinder, and bricks. From the critical analysis of the plotted results, the temperature declines against higher  $\phi$ . The physical reason behind the decrement in the temperature is that due to higher volume fraction, the colloidal fluid becomes more denser, and the collision between the fluid particles reduces which leads to decrement in the temperature. The results for temperature against higher Prandtl number values are shown in Figure 5(b) over the domain of interest. The temperature field  $\beta(\eta)$  significantly rises for multiple values of Prandtl number. At the lower end ( $\eta = 0$ ), the temperature significantly increases. The

TABLE 1: The results for  $F(\eta)$  and  $\theta(\eta)$ .

$\eta \downarrow$	$F(\eta)$			$\theta(\eta)$		
	VPM	Numerical	Error	VPM	Numerical	Error
0.0	0.000	0.000	0.000	1.031	1.031	$1.749 \times 10^{-7}$
0.1	0.140	0.140	$4.178 \times 10^{-9}$	1.031	1.031	$1.749 \times 10^{-7}$
0.2	0.279	0.279	$3.535 \times 10^{-9}$	1.031	1.031	$1.775 \times 10^{-7}$
0.3	0.413	0.413	$1.804 \times 10^{-9}$	1.030	1.030	$1.761 \times 10^{-7}$
0.4	0.541	0.541	$2.077 \times 10^{-9}$	1.030	1.030	$1.766 \times 10^{-7}$
0.5	0.661	0.661	$2.763 \times 10^{-9}$	1.029	1.029	$1.771 \times 10^{-7}$
0.6	0.769	0.769	$2.745 \times 10^{-9}$	1.028	1.028	$1.761 \times 10^{-7}$
0.7	0.861	0.861	$2.208 \times 10^{-9}$	1.025	1.025	$1.703 \times 10^{-7}$
0.8	0.934	0.934	$1.634 \times 10^{-9}$	1.020	1.020	$1.495 \times 10^{-7}$
0.9	0.982	0.982	$8.843 \times 10^{-9}$	1.013	1.013	$9.747 \times 10^{-7}$
1.0	1.000	1.000	0.000	0.999	1.000	$3.000 \times 10^{-10}$

FIGURE 2: The velocity against  $M$ . (a)  $F(\eta)$ . (b)  $F'(\eta)$ .FIGURE 3: The velocity against  $\phi$ . (a)  $F(\eta)$ . (b)  $F'(\eta)$ .

increment in the temperature of nanofluids gradually slows down from lower to upper end of the channel. Further, the increment in  $\beta(\eta)$  prevailed for the brick-shaped nanomaterial in comparison with platelets and cylinder-shaped nanomaterial, respectively.

The temperature of Cu-H<sub>2</sub>O for increasing  $S$  and  $M$  is plotted in Figures 6(a) and 6(b), respectively. It is worthy to mention that the plates move apart for  $S > 0$ . The fluid

temperature declines for higher values of  $S$ . Physically, when the upper plate moves apart from the lower one, then the flowing area increases, which reduces the collisions between the fluid particles, and consequently, the temperature  $\beta(\eta)$  drops. The temperature in Cu-H<sub>2</sub>O containing platelet-shaped Cu declines abruptly than those cylinder- and brick-shaped nanofluids. This behavior of the temperature is due to the thermophysical parameters of the Cu nanoparticles.

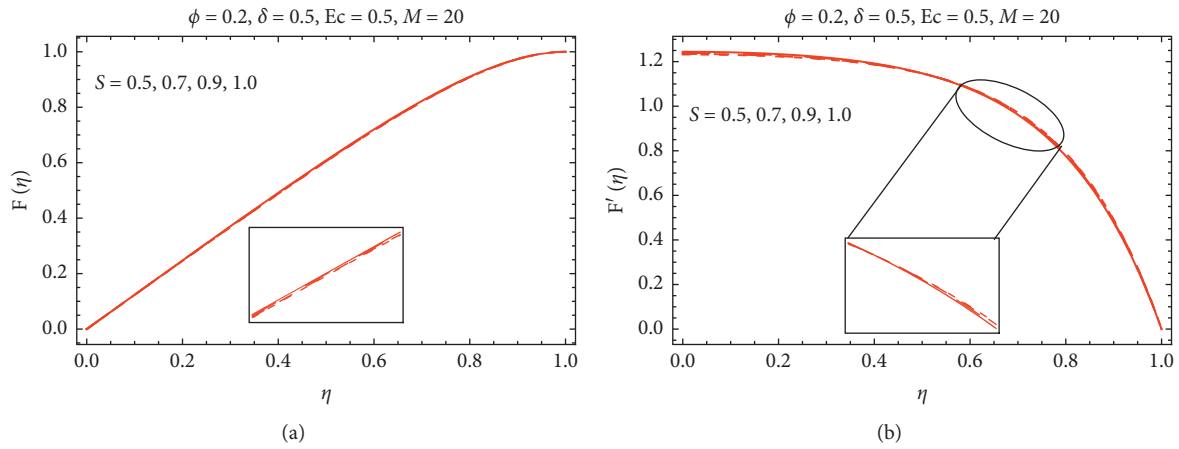


FIGURE 4: The velocity against  $S$ . (a)  $F(\eta)$ . (b)  $F'(\eta)$ .

TABLE 2: Attributes of tiny particles and regular liquid [26].

	$\rho$ (kg/m <sup>3</sup> )	$C_p$ (J/kgK)	$k$ (W/mk)	$\sigma$ ( $\Omega$ m)
Pure water	997.1	4179	0.613	0.05
Copper (Cu)	8933	385	401	$596 \times 10^7$

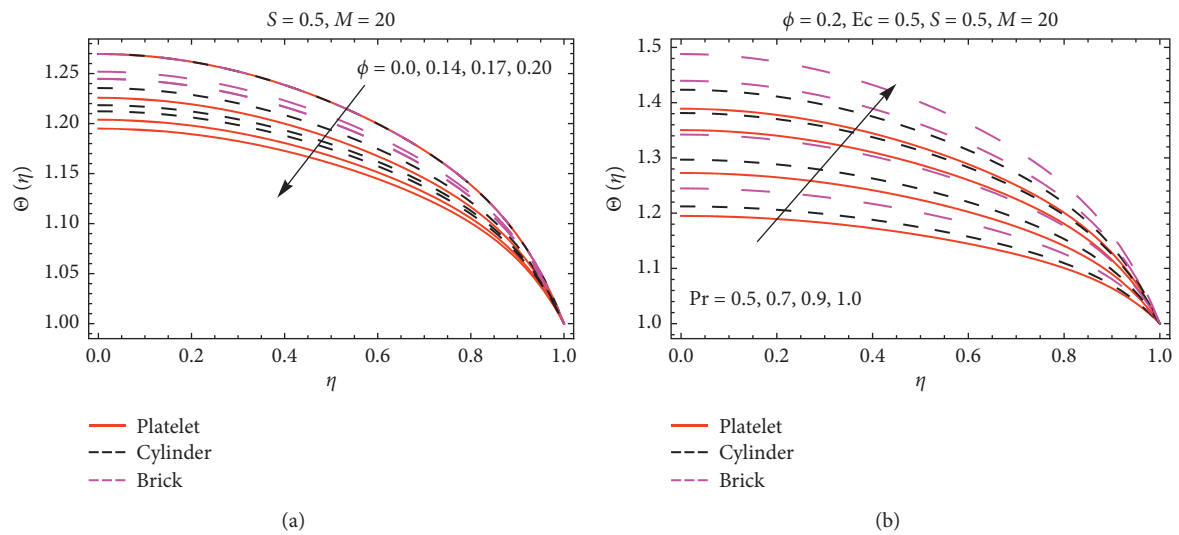


FIGURE 5: Thermal behavior  $\theta(\eta)$  against (a)  $\phi$  and (b)  $Pr$ .

The temperature field  $\beta(\eta)$  for the applied magnetic field is presented in Figure 6(b). The motion of the nanofluids reduces due to the imposed magnetic field; as a result, the fluid temperature reduces. Physically, due to perpendicularly imposed magnetic field strength, collisions between the particles reduce; consequently, the temperature drops. In the vicinity of the plates, the temperature declines very rapidly due to stronger magnetic field effects there.

The effects of viscous dissipation on  $\beta(\eta)$  are demonstrated in Figure 7(a) over the desired domain. It is examined that the temperature significantly rises due to stronger dissipation effects. The physical reason is that the internal energy of the fluid particles rises due to dissipation; as a result, the temperature rises significantly. For the nanofluid composed by brick-shaped Cu, more rapid increment in the

temperature is examined. The effects are prominent near the lower plate. The temperature  $\beta(\eta)$  variations against  $\delta$  are plotted in Figure 7(b). It is noticed that the temperature promptly rises by increasing  $\delta$ . The dominating behavior of the temperature is observed for the nanofluid containing brick-shaped Cu nanoparticles.

The impact of  $\phi$ , magnetic parameter, and  $S$  on the shear stresses is plotted in Figures 8 and 9, respectively. From the analysis, it is examined that the shear stresses drop against high volume fraction and stronger magnetic field effects. It is also observed that when the upper plate accelerates apart from the lower one, then the shear stresses decline.

Figure 10 presents the local heat transfer rate for multiple  $\phi$  values and Eckert number. From Figure 10(a), it is noticeable that the local heat transfer rate rises against high

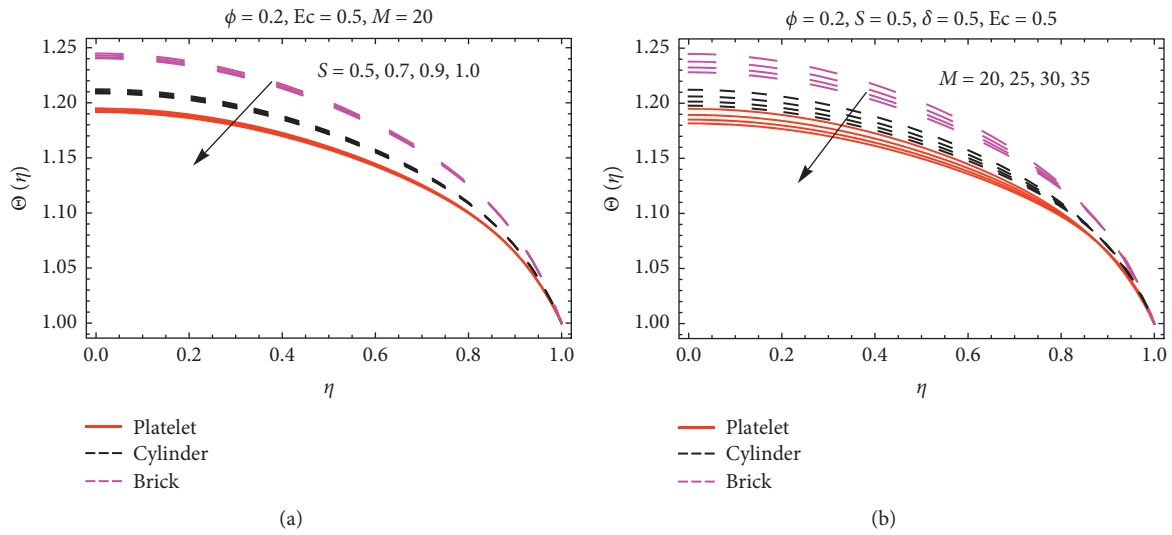


FIGURE 6: Thermal behavior  $\theta(\eta)$  against (a)  $S$  and (b)  $M$ .

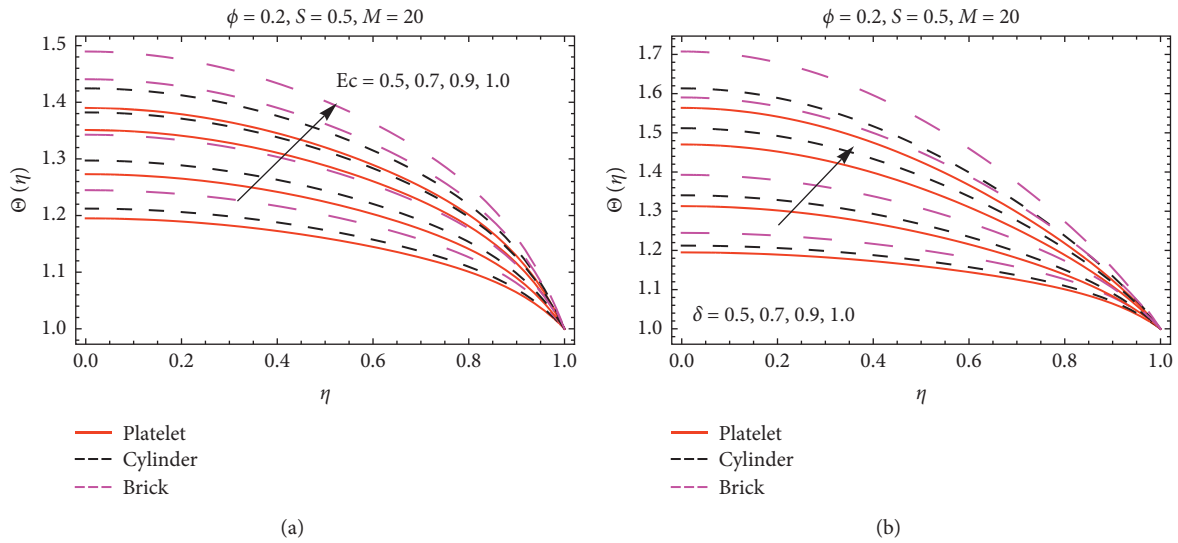


FIGURE 7: Thermal behavior  $\theta(\eta)$  against (a)  $Ec$  and (b)  $\delta$ .

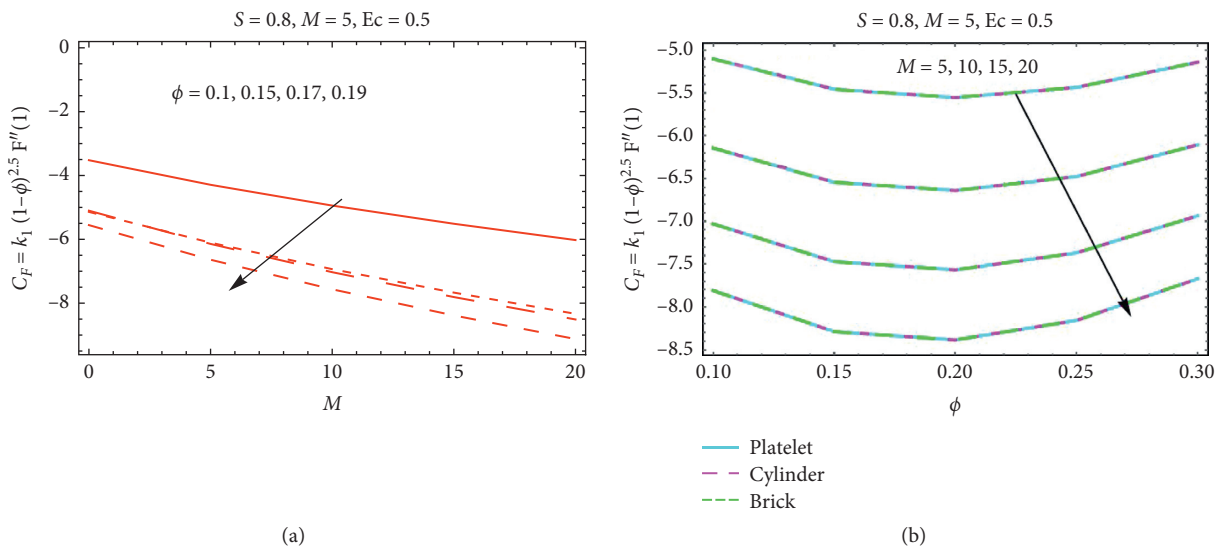


FIGURE 8: Skin friction against (a)  $\phi$  and (b)  $M$ .



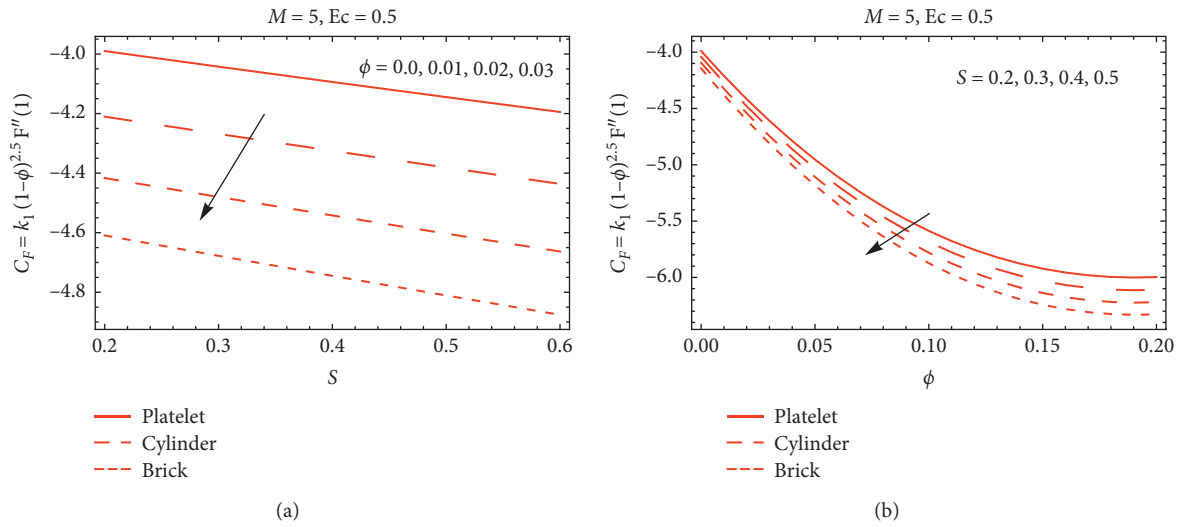


FIGURE 9: Skin friction against (a)  $\phi$  and (b)  $S$ .

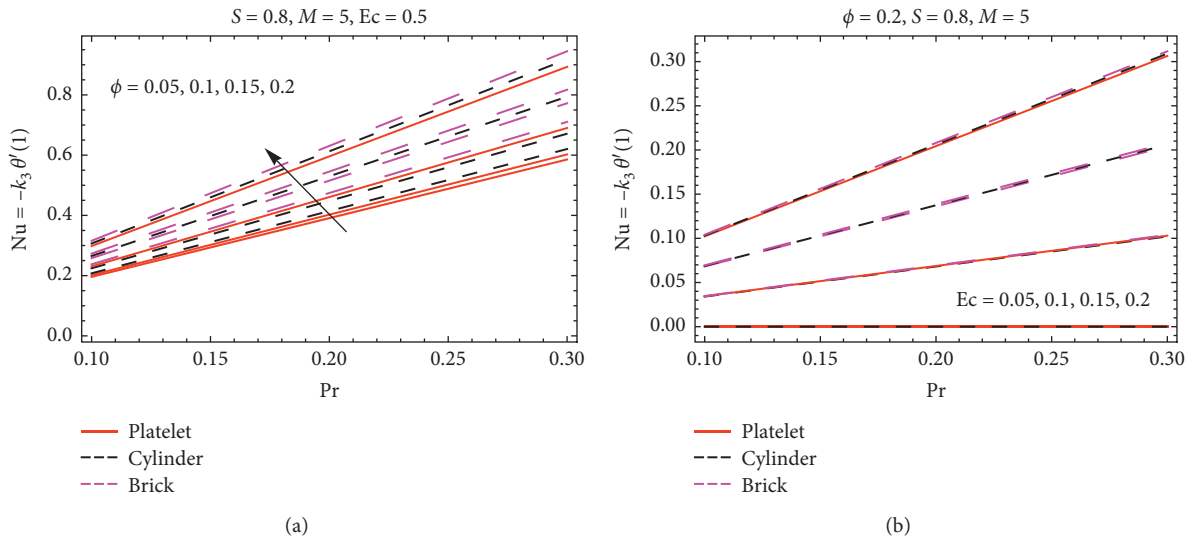
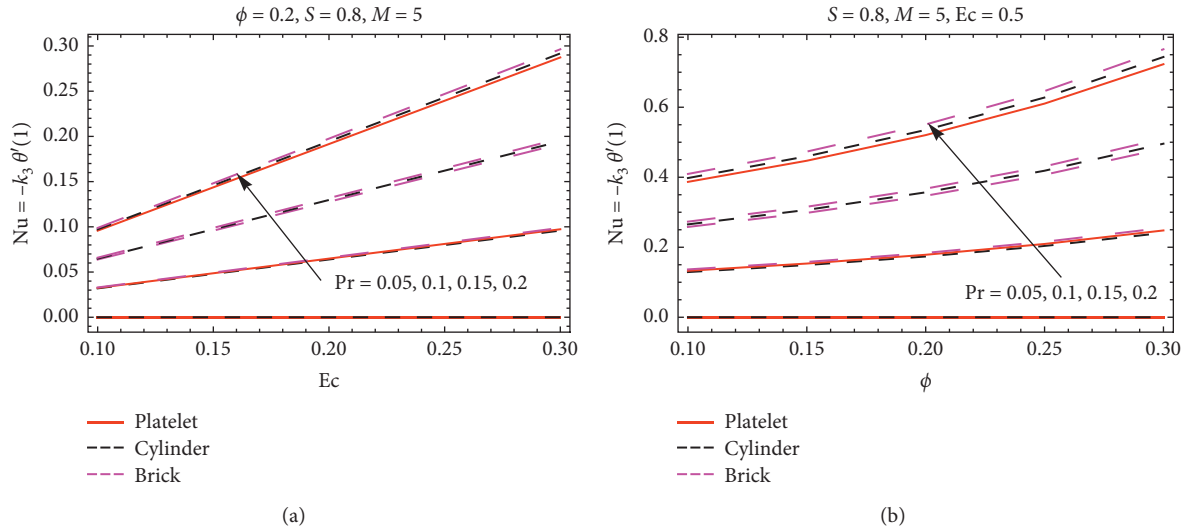


FIGURE 10: Nusselt number against (a)  $\phi$  and (b)  $Ec$ .

volume fraction. Physically, the volume fraction enhances the thermal conductance, which significantly plays the role in the local heat transfer rate. Due to high thermal conductance of bricks nanomaterial, the local heat transfer rate prevailed in comparison with platelets and cylinder nanomaterial-based nanofluids. Figure 10(b) describes the local heat transfer for increasing  $Ec$ . It is pertinent that due to high dissipation, internal energy in the nanofluid rises due to which the local thermal performance rate rises. The local heat transfer rate is slow for platelets' nanomaterial-based

nanofluids, while larger amount of heat transfer is noticed against bricks' nanomaterial-based nanofluids. Similarly, Figure 11 shows the increasing behavior of the local heat transfer against Prandtl variations.

Table 3 presents the comparative analysis between the present and existing science literature. From the comparison, it is revealed that the presented results are aligned with existing results which proves the reliability of the implemented technique and shows that the presented results are acceptable.

FIGURE 11: Nusselt number against (a)  $Pr$  and (b)  $\phi$ .TABLE 3: Comparison of  $F(\eta)$  with existing scientific literature for  $S = 1, Pr = 6.2, \delta = 0.01, M = 0, Ec = 0.01$ , and  $\phi = 0.02$ .

$\eta$	Present		Sheikholeslami et al. [11]	
	VPM	Numerical	ADM	Numerical
0.0	0.000	0.000	0.000	0.000
0.1	0.141	0.141	0.141	0.141
0.2	0.280	0.280	0.280	0.280
0.3	0.415	0.415	0.415	0.415
0.4	0.544	0.544	0.544	0.544
0.5	0.663	0.663	0.663	0.663
0.6	0.771	0.771	0.771	0.771
0.7	0.863	0.863	0.863	0.863
0.8	0.935	0.935	0.935	0.935
0.9	0.982	0.982	0.982	0.982
1.0	1.000	1.000	1.000	1.000

## 4. Conclusions

An analytical investigation of the Cu nanomaterial-based nanofluid between parallel rotating sheets is conducted. The colloidal model is tackled analytically, and the results are plotted against the pertinent flow parameters. From the critical analysis of attained results, it is noticed that the temperature of the nanofluid declines against higher volumetric fraction and abruptly increases for the Prandtl number. These effects are prominent near the surface and gradually become slow apart from the plates. Moreover, the stronger viscous dissipation effects lead to the increment in the temperature of the nanofluid. The local rate of heat transfer significantly rises for brick-shaped nanoparticles. Finally, it is observed that the nanofluid is better for industrial uses due to its prominent heat transfer properties. The analysis is confined to the Newtonian host liquid; otherwise, the model will be not valid. A comparative analysis aligned the presented study with existing science literature.

## Data Availability

The data used to support the findings of the study are available from the corresponding author upon request.

## Conflicts of Interest

The authors declare that there are no conflicts of interest regarding the publication of this paper.

## References

- [1] M. J. Stefan, "Versuch Uber die scheinbare adhesion," *Mathematisch-Naturwissenschaftliche*, vol. 69, 1874.
- [2] M. Mustafa, T. Hayat, and S. Obaidat, "On heat and mass transfer in the unsteady squeezing flow between parallel plates," *Meccanica*, vol. 47, no. 7, pp. 1581–1589, 2012.
- [3] G. Domairry and A. Aziz, "Approximate analysis of MHD squeeze flow between two parallel disks with suction or injection by homotopy perturbation method," *Mathematical Problems in Engineering*, vol. 2009, Article ID 603916, 2009.
- [4] U. Khan, N. Ahmed, and S. T. Mohyud-Din, "Analysis of magnetohydrodynamic flow and heat transfer of Cu-water nanofluid between parallel plates for different shapes of nanoparticles," *Neural Computing and Applications*, vol. 29, no. 10, pp. 695–703, 2018.
- [5] S. Mohyud-Din, U. Khan, N. Ahmed, and S. Hassan, "Magnetohydrodynamic flow and heat transfer of nanofluids in stretchable convergent/divergent channels," *Applied Sciences*, vol. 5, no. 4, pp. 1639–1664, 2015.
- [6] S. U. S. Choi, "Enhancing thermal conductivity of fluids with nanoparticles," in *Developments and applications of non-Newtonian flows. ASME FED*, 231/MD66, D. A. Siginer and H. P. Wang, Eds., pp. 99–105, 1995.
- [7] S. U. S. Choi, Z. G. Zhang, W. Yu, F. E. Lockwood, and E. A. Grulke, "Anomalous thermal conductivity enhancement in nanotube suspensions," *Applied Physics Letters*, vol. 79, no. 14, pp. 2252–2254, 2001.

- [8] H. Ş. Aybar, M. Sharifpur, M. R. Azizian, M. Mehrabi, and J. P. Meyer, "A review of thermal conductivity models for nanofluids," *Heat Transfer Engineering*, vol. 36, no. 13, pp. 1085–1110, 2015.
- [9] S. Göktepe, K. Ertürk, and H. Ertürk, "Comparison of single and two-phase models for nanofluid convection at the entrance of a uniformly heated tube," *International Journal of Thermal Sciences*, vol. 80, pp. 83–92, 2014.
- [10] N. Hedayati and A. Ramiar, "Investigation of two phase unsteady nanofluid flow and heat transfer between moving parallel plates in the presence of magnetic field using GM," *Nano Micro Scale Sci. Tech.* vol. 4, no. 2, pp. 47–53, 2016.
- [11] M. Sheikholeslami, D. D. Ganji, and H. R. Ashorynejad, "Investigation of squeezing unsteady nanofluid flow using ADM," *Powder Technology*, vol. 239, pp. 259–265, 2013.
- [12] M. Sheikholeslami, T. Hayat, and A. Alsaedi, "MHD free convection of Al<sub>2</sub>O<sub>3</sub>-water nanofluid considering thermal radiation: a numerical study," *International Journal of Heat and Mass Transfer*, vol. 96, pp. 513–524, 2016.
- [13] M. Sheikholeslami and M. M. Rashidi, "Non-uniform magnetic field effect on nanofluid hydrothermal treatment considering Brownian motion and thermophoresis effects," *Journal of the Brazilian Society of Mechanical Sciences and Engineering*, vol. 38, no. 4, pp. 1171–1184, 2016.
- [14] M. Sheikholeslami and A. J. Chamkha, "Flow and convective heat transfer of a ferro-nanofluid in a double-sided lid-driven cavity with a wavy wall in the presence of a variable magnetic field," *Numerical Heat Transfer, Part A: Applications*, vol. 69, no. 10, pp. 1186–1200, 2016.
- [15] A. S. Dogonchi, K. Divsalar, and D. D. Ganji, "Flow and heat transfer of MHD nanofluid between parallel plates in the presence of thermal radiation," *Computer Methods in Applied Mechanics and Engineering*, vol. 310, pp. 58–76, 2016.
- [16] M. Sheikholeslami and D. D. Ganji, "Nanofluid flow and heat transfer between parallel plates considering Brownian motion using DTM," *Computer Methods in Applied Mechanics and Engineering*, vol. 283, pp. 651–663, 2014.
- [17] M. Sheikholeslami, M. M. Rashidi, D. M. Al Saad, F. Firouzi, H. B. Rokni, and G. Domairry, "Steady nanofluid flow between parallel plates considering thermophoresis and Brownian effects," *Journal of King Saud University-Science*, vol. 28, no. 4, pp. 380–389, 2016.
- [18] S. T. Mohyud-Din, Z. A. Zaidi, U. Khan, and N. Ahmed, "On heat and mass transfer analysis for the flow of a nanofluid between rotating parallel plates," *Aerospace Science and Technology*, vol. 46, pp. 514–522, 2015.
- [19] K. Singh, S. K. Rawat, and M. Kumar, "Heat and mass transfer on squeezing unsteady MHD nanofluid flow between parallel plates with slip velocity effect," *Journal of Nanoscience*, vol. 2016, Article ID 9708562, 11 pages, 2016.
- [20] S. T. Mohyud-Din, Adnan, U. Khan et al., "Thermal transport investigation in magneto-radiative GO-MoS<sub>2</sub>/H<sub>2</sub>O-C<sub>2</sub>H<sub>6</sub>O<sub>2</sub> hybrid nanofluid subject to cattaneo-christov model," *Molecules*, vol. 25, no. 11, Article ID 2592, 2020.
- [21] S. Z. A. Adnan, S. Z. A. Zaidi, U. Khan et al., "Impacts of freezing temperature based thermal conductivity on the heat transfer gradient in nanofluids: applications for a curved rigid surface," *Molecules*, vol. 25, no. 9, Article ID 2152, 2020.
- [22] N. Ahmed, Adnan, U. Khan et al., "Radiative colloidal investigation for thermal transport by incorporating the impacts of nanomaterial and molecular diameters (dNanoparticles, dFluid): applications in multiple engineering systems," *Molecules*, vol. 25, no. 8, Article ID 1896, 2020.
- [23] Z. Shah, S. Islam, H. Ayaz, and S. Khan, "Radiative heat and mass transfer analysis of micropolar nanofluid flow of casson fluid between two rotating parallel plates with effects of Hall current," *Journal of Heat Transfer*, vol. 141, no. 2, 2019.
- [24] U. Khan, Adnan, N. Ahmed et al., " $\gamma$ -Nanofluid thermal transport between parallel plates suspended by micro-cantilever sensor by incorporating the effective Prandtl model: applications to biological and medical sciences," *Molecules*, vol. 25, no. 8, p. 1777, 2020.
- [25] T. Gul, M. Z. Ullah, A. K. Alzahrani, and I. S. Amiri, "Thermal performance of the graphene oxide nanofluids flow in an upright channel through a permeable medium," *IEEE Access*, vol. 7, pp. 102345–102355, 2019.
- [26] N. S. Akbar and A. W. Butt, "Ferromagnetic effects for peristaltic flow of Cu-water nanofluid for different shapes of nanosize particles," *Applied Nanoscience*, vol. 6, no. 3, pp. 379–385, 2016.
- [27] R. Ellahi, M. Hassan, A. Zeeshan, and A. A. Khan, "The shape effects of nanoparticles suspended in HFE-7100 over wedge with entropy generation and mixed convection," *Applied Nanoscience*, vol. 6, no. 5, pp. 641–651, 2016.
- [28] W. Sikandar, U. Khan, N. Ahmed, and S. T. Mohyud-Din, "Variation of parameters method with an auxiliary parameter for initial value problems," *Ain Shams Engineering Journal*, vol. 9, no. 4, pp. 1959–1963, 2018.